25. Solntseva, M. P. in *Comparative Embryology of Flowering Plants* (ed. Yakovlev, M. S.) 51–54 (Nauka, Leningrad, Russia, 1981) (in Russian).
26. Tobe, H., Jaffre, T. & Raven, P. H. Embryology of *Amborella* (Amborellaceae): descriptions and polarity of character states. *J. Plant Res.* **113,** 271–280 (2000).
27. Wilson, M. F. & Burley, N. *Mate Choice in Plants: Tactics, Mechanisms, and Consequences* (Princeton Univ. Press, Princeton, 1983).
28. Queller, D. C. in *Oxford Surveys in Evolutionary Biology* (eds Harvey, P. H. & Partridge, L.) 73–109 (Oxford Univ. Press, Oxford, 1989).
29. Chaw, S. M., Parkinson, C. L., Cheng, Y., Vincent, T. M. & Palmer, J. D. Seed plant phylogeny inferred from all three plant genomes: Monophyly of extant gymnosperms and origin of Gnetales from conifers. *Proc. Natl Acad. Sci. USA* **97,** 4086–4091 (2000).
30. Bowe, L. M., Coat, G. & dePamphilis, C. W. Phylogeny of seed plants based on all three genomic compartments: Extant gymnosperms are monophyletic and Gnetales' closest relatives are conifers. *Proc. Natl Acad. Sci. USA* **97,** 4092–4097 (2000).

Supplementary Information accompanies the paper on *Nature*'s website (http://www.nature.com).

Acknowledgements

We thank P. K. Diggle, L. Hufford and R. H. Robichaux for critical comments on the manuscript and W. Gallup and M. Dozier for assistance with histology. This work was supported by grants from the National Science Foundation to W.E.F.

Competing interests statement

The authors declare that they have no competing financial interests.

Correspondence and requests for materials should be addressed to W.E.F. (e-mail: ned@colorado.edu).

Mechanism for the learning deficits in a mouse model of neurofibromatosis type 1

Rui M. Costa*, Nikolai B. Federov*†, Jeff H. Kogan*†, Geoffrey G. Murphy*, Joel Stern*, Masuo Ohno*, Raju Kucherlapati‡, Tyler Jacks§ & Alcino J. Silva*

** Departments of Neurobiology, Psychiatry and Psychology, BRI, University of California at Los Angeles, Los Angeles, California 90095-1761, USA*
‡ Department of Molecular Genetics, Albert Einstein College of Medicine, 1300 Morris Park Avenue, Bronx, New York, New York 10461, USA
§ Department of Biology, Massachusetts Institute of Technology, Cambridge, Massachusetts 02139, USA

Neurofibromatosis type I (NF1) is one of the most common single-gene disorders that causes learning deficits in humans[1]. Mice carrying a heterozygous null mutation of the *Nf1* gene (*Nf1*$^{+/-}$) show important features of the learning deficits associated with NF1 (ref. 2). Although neurofibromin has several known properties and functions, including Ras GTPase-activating protein activity[3,4], adenylyl cyclase modulation[5,6] and microtubule binding[7], it is unclear which of these are essential for learning in mice and humans. Here we show that the learning deficits of *Nf1*$^{+/-}$ mice can be rescued by genetic and pharmacological manipulations that decrease Ras function. We also show that the *Nf1*$^{+/-}$ mice have increased GABA (γ-amino butyric acid)-mediated inhibition and specific deficits in long-term potentiation, both of which can be reversed by decreasing Ras function. Our results indicate that the learning deficits associated with NF1 may be caused by excessive Ras activity, which leads to impairments in long-term potentiation caused by increased GABA-mediated inhibition. Our findings have implications for the development of treatments for learning deficits associated with NF1.

† Present address: Memory Pharmaceuticals Corporation, 100 Philips Parkway, Montvale, New Jersey 07645, USA.

Visual–spatial problems are among the most common cognitive deficits detected in individuals affected with NF1 (refs 1, 8). Studies have shown that *Nf1*$^{+/-}$ mice have abnormal spatial learning[2] when tested in the hidden version of the water maze—a task that is sensitive to hippocampal lesions[9]. Studies suggest that an upregulation of Ras activity may account for the learning deficits in NF1 both in mice[10] and humans[11]. To test this hypothesis, we crossed the *Nf1*$^{+/-}$ mice (C57B6/N background) with mice heterozygous for a null mutation in the *K-ras* gene[12] (*K-ras*$^{+/-}$, 129T2/SvEmsJ), and tested the F_1 descendants (hybrid isogenic background) in the hidden version of the water maze task. Because *K-ras*$^{-/-}$ mice, like *Nf1*$^{-/-}$ (ref. 13), die *in utero*[12], we used *K-ras*$^{+/-}$ mice, which are viable and show no apparent developmental defects.

Mice were trained with two trials per day. In all the following experiments, no differences between genotypes and/or treatments were observed in acquisition (Fig. 1a, d, g), floating, thigmotaxic behaviour or swimming speed (data not shown). Spatial learning was assessed in a probe trial[14] (training day 7), in which the platform was removed from the pool. The time spent searching in the training quadrant was different among the different genotypes (analysis of variance, ANOVA, $F_{3,61} = 7.27$, $P < 0.05$). Wild-type mice spent significantly more time searching in the training quadrant than did *Nf1*$^{+/-}$ mice (Fisher's protected least significant difference, PLSD, $P < 0.05$; Fig. 1b), confirming that the *Nf1*$^{+/-}$ mice have impaired spatial learning. *K-ras*$^{+/-}$ mice were also impaired ($P < 0.05$; Fig. 1b); however, mice carrying heterozygous mutations in both the *Nf1* and the *K-ras* genes (*Nf1*$^{+/-}$/*K-ras*$^{+/-}$) spent as much time as wild-type mice in the training quadrant ($P > 0.05$; Fig. 1b), and significantly more time than *Nf1*$^{+/-}$ and *K-ras*$^{+/-}$ mice ($P < 0.05$). This indicates that the learning deficits in *Nf1*$^{+/-}$ mice can be rescued by the *K-ras*$^{+/-}$ mutation. Furthermore, both wild-type (paired *t*-test, $t_{23} = 5.935$, $P < 0.05$) and *Nf1*$^{+/-}$/*K-ras*$^{+/-}$ mice searched selectively for the missing platform; that is, they searched closer to the exact platform position than to the opposite position in the pool[15] ($t_{10} = 4.09$, $P < 0.05$; Fig. 1c), whereas *Nf1*$^{+/-}$ and *K-ras*$^{+/-}$ mice did not (*Nf1*$^{+/-}$ $t_{14} = 1.83$; *K-ras*$^{+/-}$ $t_{14} = 0.149$; $P > 0.05$).

Mutations that decrease Ras function do rescue the deficits of the *Nf1*$^{+/-}$ mice because a null heterozygous mutation in *N-ras* (*N-ras*$^{+/-}$), another mammalian *ras* gene with overlapping function and similar expression to that of *K-ras*[12], also reverses the spatial learning deficits of the *Nf1*$^{+/-}$ mice (Fig. 1e, f; see Methods). During the probe trial, there was a significant effect of genotype on searching strategy ($F_{3,32} = 2.83$, $P < 0.05$; Fig. 1e). *Nf1*$^{+/-}$/*N-ras*$^{+/-}$ mice were indistinguishable from wild type (Fisher's PLSD, $P > 0.05$), and searched significantly more in the training quadrant than did *Nf1*$^{+/-}$ mice ($P < 0.05$). Also, analysis of proximity scores showed that both wild-type and *Nf1*$^{+/-}$/*N-ras*$^{+/-}$ mice searched selectively (wild type, $t_9 = 3.621$; *Nf1*$^{+/-}$/*N-ras*$^{+/-}$, $t_8 = 5.84$; $P < 0.05$; Fig. 1f), whereas *Nf1*$^{+/-}$ mice did not ($t_{14} = 1.83$, $P > 0.05$). The *N-ras*$^{+/-}$ mutation by itself did not produce any detectable phenotype ($P > 0.05$; Fig. 1e), consistent with previous studies indicating that Ras signalling is less impaired in *N-ras* than in *K-ras* mutants[12].

The *ras* mutations that reversed the *Nf1*$^{+/-}$ spatial learning deficits should result in a decrease in Ras function throughout the life of the mice. To determine whether decreases in Ras function specifically during training could reverse the learning deficits of the *Nf1*$^{+/-}$ mice, we used a farnesyl-transferase inhibitor (FTI; BMS 191563; ref. 16). This agent reduces Ras signalling by blocking farnesylation, a post-translational modification that is essential for Ras function[17]. FTIs have been shown to rescue other NF1 phenotypes, such as Schwann cell proliferation in human and murine cells[18,19]. Wild-type and *Nf1*$^{+/-}$ mice were injected intraperitoneally every day 60 min before training with either saline or 5 mg per kg (body weight) BMS 191563; the training conditions and the genetic background of the animals were the same as in the *Nf1*$^{+/-}$/*K-ras*$^{+/-}$ experiment.

Analysis of the day 7 probe trial showed an effect of genotype–

treatment interaction on searching strategy ($F_{3,32} = 2.83$, $P < 0.05$; Fig. 1h). *Nf1*$^{+/-}$ mice treated with BMS191563 searched significantly longer in the training quadrant than *Nf1*$^{+/-}$ mice treated with saline ($P < 0.05$), and were indistinguishable from wild-type mice ($P > 0.05$). Moreover, analysis of proximity scores showed that *Nf1*$^{+/-}$ mice treated with BMS191563 searched selectively ($t_{18} = 4.13$, $P < 0.05$; Fig. 1i), as did wild-type mice ($t_{17} = 4.33$, $P < 0.05$), whereas *Nf1*$^{+/-}$ mice treated with saline did not ($t_{19} = 0.266$, $P > 0.05$). Administration of 5 mg per kg BMS191563 did not adversely affect wild-type animals, as these mice searched equivalently to wild-type mice treated with saline ($P > 0.05$; Fig. 1h). The finding that the learning deficits of *Nf1*$^{+/-}$ mice can be reversed with an FTI confirms our genetic results, and shows that these learning deficits are reversible in adult mice.

Learning is thought to occur through activity-dependent synaptic modifications in neuronal networks[20]. To determine whether changes in synaptic plasticity might account for the spatial (hippocampal-dependent[9]) learning impairments of *Nf1*$^{+/-}$ mutants, we examined long-term potentiation (LTP) at Schaffer collateral/CA1 synapses in hippocampal slices from these mice. Schaffer collateral stimulation (60 μA) elicited a similar baseline excitatory postsynaptic potential (EPSP) in *Nf1*$^{+/-}$ and wild-type mice (*Nf1*$^{+/-}$ = 1.02 ± 0.06 mV, wild type = 1.09 ± 0.05, $F_{1,54} = 0.58$, $P > 0.05$).

We first induced LTP using a theta-burst stimulation (TBS) protocol, which mimics the *in vivo* activity of hippocampal neurons during exploratory behaviour[21]. This protocol consisted of two, five or ten bursts. The two-burst protocol elicited a persistent potentiation in wild-type animals (Fig. 2a), which was significantly larger than that triggered in *Nf1*$^{+/-}$ mice ($F_{1,11} = 6.98$, $P < 0.05$). This difference was also seen with five ($F_{1,13} = 8.27$, $P < 0.05$; Fig. 2b) and ten bursts ($F_{1,16} = 6.93$, $P < 0.05$; Fig. 2c). Thus, TBS stimulation shows that there is an LTP deficit in *Nf1*$^{+/-}$ mice (Fig. 2e). We also examined LTP induced under high-frequency stimulation (HFS, 100 Hz for 1 s; Fig. 2e). With this protocol, the potentiation induced was equivalent in wild-type and *Nf1*$^{+/-}$ mice ($F_{1,15} = 0.06$, $P > 0.05$; see below).

To determine whether the TBS-induced LTP deficits in *Nf1*$^{+/-}$ mice were caused by increased Ras function, we tested *Nf1*$^{+/-}$/*K-ras*$^{+/-}$ mice (of the same genetic background as those tested in the water maze). The magnitude of CA1 LTP induced with a two-burst protocol differed across genotypes ($F_{3,35} = 4.6$, $P < 0.05$; Fig. 2d). The amount of LTP induced in *Nf1*$^{+/-}$/*Kras*$^{+/-}$ was significantly higher than that induced in *Nf1*$^{+/-}$ mice (Fisher PLSD, $P < 0.05$), and equivalent to that of wild-type mice ($P > 0.05$; Fig. 2f). *K-ras*$^{+/-}$ mice were also significantly impaired relative to both *Nf1*$^{+/-}$/*Kras*$^{+/-}$ and wild-type mice (LTP at 40 min 114 ± 4.47, $P < 0.05$; data not shown). These results show that the *K-ras*$^{+/-}$ mutation can rescue the LTP deficits in *Nf1*$^{+/-}$ mice, just as it can also rescue their spatial learning deficits.

Nf1$^{+/-}$ mice also showed a decrease in the input–output function

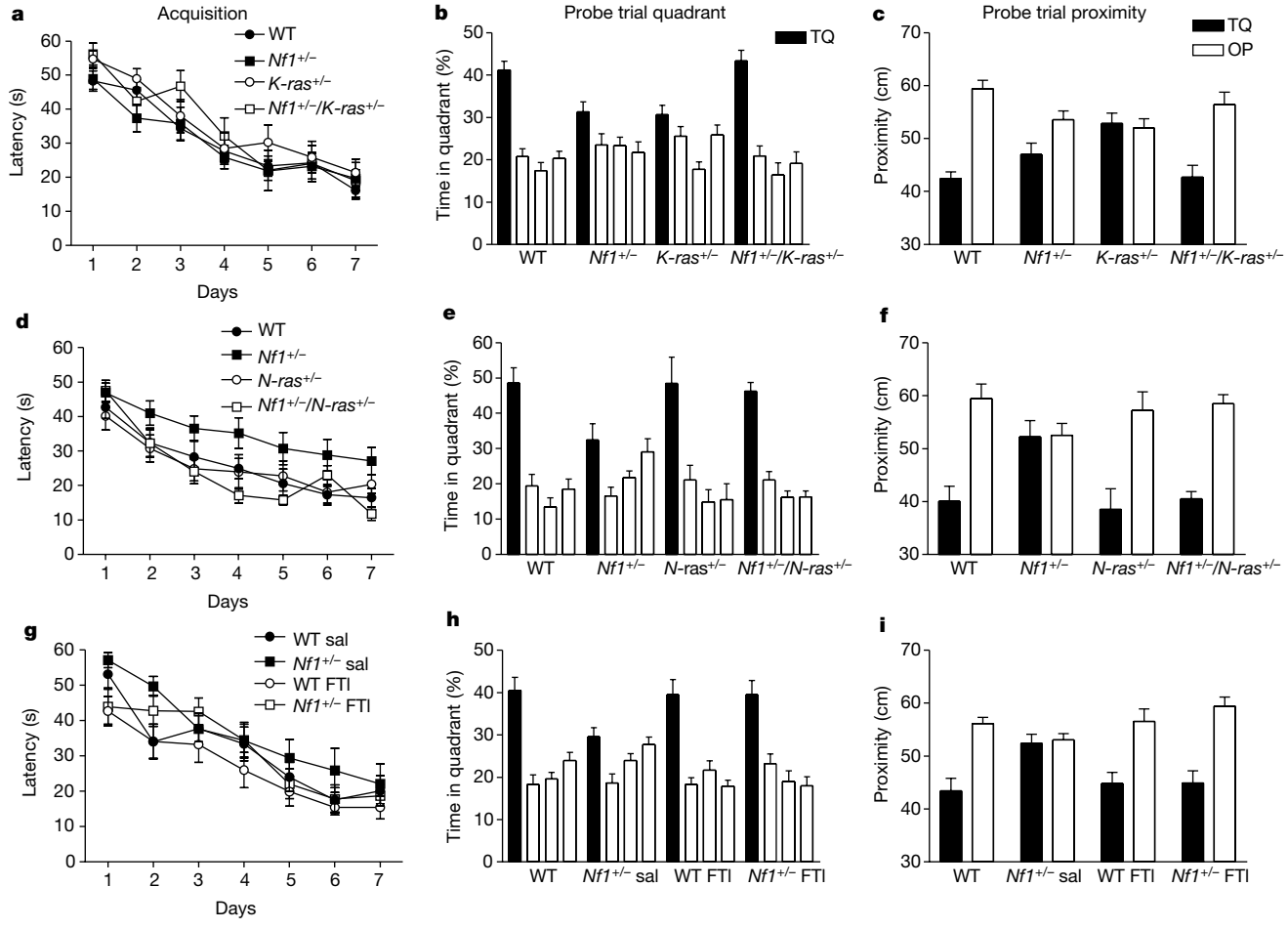

Figure 1 Learning deficits of *Nf1*$^{+/-}$ mice are Ras dependent. **a**–**c**, Hidden version of the water maze for the *Nf1*$^{+/-}$/*K-ras*$^{+/-}$ population (wild type (WT), $n = 24$; *Nf1*$^{+/-}$, $n = 15$; *K-ras*$^{+/-}$, $n = 15$; *Nf1*$^{+/-}$/*K-ras*$^{+/-}$, $n = 11$). **a**, Latency to get to the platform over days. **b**, Per cent time spent in each quadrant during a probe trial **c**, Average proximity to the exact position where the platform was during training, compared with proximity to the opposite position in the pool. **d**–**f**, Acquisition, per cent time in quadrant, and proximity data for the *Nf1*$^{+/-}$/*N-ras*$^{+/-}$ population (WT, $n = 10$; *Nf1*$^{+/-}$, $n = 10$; *N* − *ras*$^{+/-}$, $n = 7$; *Nf1*$^{+/-}$/*N-ras*$^{+/-}$, $n = 9$). **g**–**i**, Acquisition, per cent time in quadrant, and proximity data for the different genotypes and treatments during the FTI rescue experiment (WT_{FTI}, $n = 19$; WT_{saline}, $n = 18$; $Nf1^{+/-}_{FTI}$, $n = 18$; $Nf1^{+/-}_{saline}$, $n = 18$). Quadrants are training quadrant (TQ), adjacent right, adjacent left and opposite quadrant (OP).

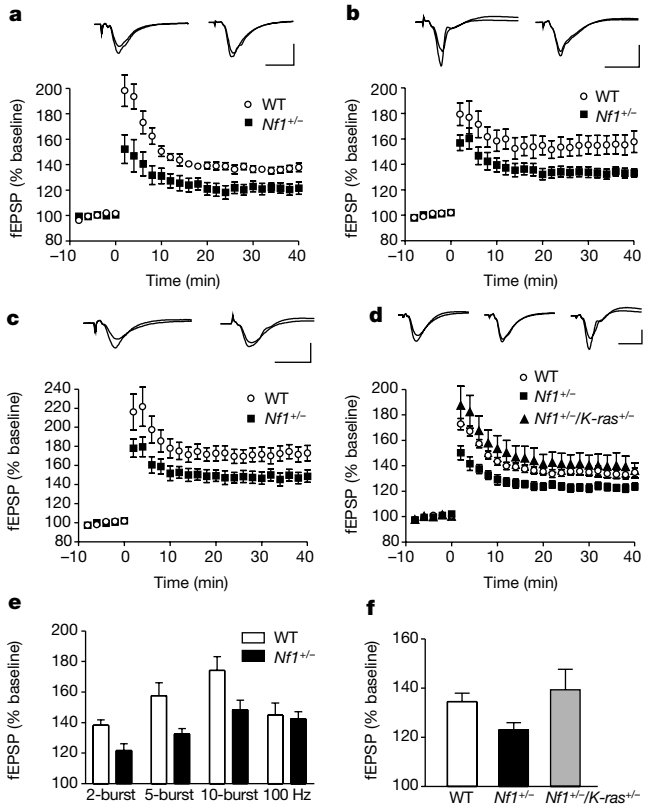

Figure 2 Ras-dependent long-term potentiation deficits in *Nf1*$^{+/-}$ animals. Percentage of baseline field EPSP (fEPSP) is plotted over time. **a**, Two-burst induction protocol (wild type (WT), $n = 5$; *Nf1*$^{+/-}$, $n = 8$). **b**, Five-burst induction protocol (WT, $n = 7$; *Nf1*$^{+/-}$, $n = 8$). **c**, Ten-burst induction protocol (WT, $n = 7$; *Nf1*$^{+/-}$, $n = 11$). **d**, Two-burst induction protocol. LTP deficits in *Nf1*$^{+/-}$ mice are Ras dependent (WT, $n = 13$; *Nf1*$^{+/-}$, $n = 13$; *Nf1*$^{+/-}$/*K-ras*$^{+/-}$, $n = 8$). Representative traces are shown from left to right for WT, *Nf1*$^{+/-}$ and *Nf1*$^{+/-}$/*K-ras*$^{+/-}$. Horizontal bar, 10 ms; vertical bar, 1 mV. **e**, LTP measured 40 min after induction under different stimulation protocols. **f**, LTP measured 40 min after induction in the *Nf1*$^{+/-}$/*K-ras*$^{+/-}$ rescue experiment.

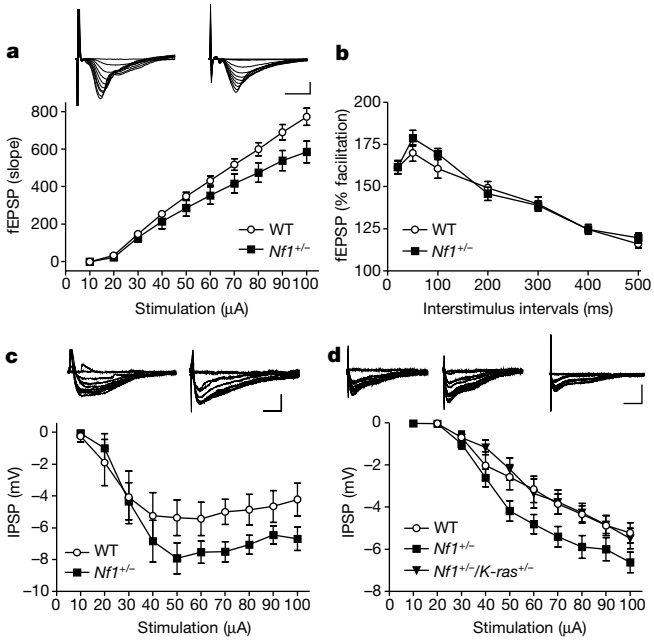

Figure 3 Ras-dependent enhanced inhibition in *Nf1*$^{+/-}$ mice. **a**, Input–output function at the CA3–CA1 synapse (wild type (WT), $n = 9$; *Nf1*$^{+/-}$, $n = 9$) with representative traces (left, WT; right, *Nf1*$^{+/-}$). Horizontal bar, 5 ms; vertical bar, 0.5 mV. **b**, Paired-pulse facilitation (WT, $n = 9$; *Nf1*$^{+/-}$, $n = 12$) at different interstimulus intervals. **c**, Evoked IPSPs measured intracellularly in CA1 pyramidal cells using different stimulation strengths (WT, 5 mice, 13 neurons, *Nf1*$^{+/-}$, 4 mice, 17 neurons). **d**, Monosynaptically evoked IPSPs measured in the presence of AP5 and CNQX (WT, 7 mice, 17 neurons; *Nf1*$^{+/-}$, 11 mice, 23 neurons; *Nf1*$^{+/-}$/*K-ras*$^{+/-}$, 6 mice, 13 neurons). **c**, **d**, Representative traces are shown left to right for WT, *Nf1*$^{+/-}$ and *Nf1*$^{+/-}$/*K-ras*$^{+/-}$ mice. Horizontal bar, 100 ms; vertical bar, 5 mV.

of extracellularly recorded EPSPs at the Schaffer collateral/CA1 synapse ($F_{1,16} = 4.11$, $P < 0.05$, Fisher PLSD (100 μA), $P < 0.05$; Fig. 3a). Neither this impairment, nor the LTP deficit, seemed to be caused by abnormal presynaptic function, because electrophysiological phenomena sensitive to presynaptic changes such as paired-pulse facilitation ($F_{1,19} = 0.43$, $P > 0.05$; Fig. 3b), augmentation, depletion and probability of glutamate release[22] were normal in *Nf1*$^{+/-}$ mice (data not shown). The LTP deficits of *Nf1*$^{+/-}$ mice were revealed by TBS, but not HFS stimulation. LTP induced by TBS is more sensitive to changes in GABA-mediated inhibition than is LTP induced by HFS[23]. In addition, Ras can affect chloride currents in adrenal gland cells[24]. We therefore investigated whether GABA-mediated inhibition was altered in *Nf1*$^{+/-}$ mice. We measured evoked inhibitory postsynaptic potentials (IPSPs) in CA1 pyramidal cells of hippocampal slices from *Nf1*$^{+/-}$ mice. We found that *Nf1*$^{+/-}$ mice have larger IPSPs than those of wild-type controls (ANOVA, $F_{1,88} = 5.31$, $P < 0.05$; Fisher PLSD, $P < 0.05$; Fig. 3c). We also measured monosynaptically evoked IPSPs in the presence of AP5 (2-amino-5-phosphonopentanoic acid), an NMDA (*N*-methyl-D-aspartate) receptor antagonist, and CNQX (6-cyano-7-nitroquinoxaline-2,3-dione), an AMPA (α-amino-3-hydroxy-5-methyl-isoxazole-4-propionic acid) receptor antagonist (Fig. 3d). Once again, IPSPs were larger in *Nf1*$^{+/-}$ than in wild-type mice (ANOVA, $F_{2,237} = 5.09$, $P < 0.05$; Fisher PLSD, $P < 0.05$; Fig. 3d). The increased inhibition in *Nf1*$^{+/-}$ mice was also rescued by manipulations that decrease Ras function: IPSPs in *Nf1*$^{+/-}$/*K-ras*$^{+/-}$ mice are smaller than in *Nf1*$^{+/-}$ mice ($P < 0.05$; Fig. 3d) and indistinguishable from wild-type controls ($P > 0.05$).

Results from several of our experiments suggest that this increase in GABA-mediated inhibition is the cause for the LTP deficits in *Nf1*$^{+/-}$ mice. First, picrotoxin (10 μM), a $GABA_A$ receptor antagonist, rescues the LTP (two-burst) deficits of *Nf1*$^{+/-}$ mice ($F_{1,9} = 0.78$, $P > 0.05$; Fig. 4a). Second, LTP deficits are evident in *Nf1*$^{+/-}$ mice (Fig. 2a) at synaptic stimulation strengths (60 μA) that cause an increase in GABA-mediated inhibition, but are absent at synaptic stimulation strengths (35 μA) that do not cause increases in inhibition ($F_{1,27} = 0.263$, $P > 0.05$; Figs 3c and 4b). Note that in wild-type mice the LTP induced at a stimulation strength of 60 μA is larger than that induced at 35 μA ($F_{1,16} = 18.1$, $P < 0.05$), whereas in *Nf1*$^{+/-}$ mice it is not ($F_{1,22} = 0.18$, $P > 0.05$; Fig. 4c). This is consistent with the larger inhibition in *Nf1*$^{+/-}$ mice at 60 μA (Fig. 4c). Third, LTP induced with HFS, which is less sensitive to inhibition than LTP induced with TBS, is normal in *Nf1*$^{+/-}$ mice (Fig. 2e).

Our results show that the spatial learning impairments in a mouse model of NF1 can be rescued by two different genetic manipulations that decrease Ras levels. Our data also show that the learning deficits in *Nf1*$^{+/-}$ mice can be reversed pharmacologically in the adult—an important finding for the development of treatments for learning deficits associated with NF1. Our results suggest that abnormally high or low Ras activity can disrupt learning, indicating that precise Ras modulation by neurofibromin is essential for learning and memory. Although the learning deficits in *Drosophila* that lack neurofibromin are dependent on adenylyl cyclase[6], *Nf1*$^{+/-}$ mice have normal adenylyl cyclase activity[25]. These mice, however, have upregulated Ras/mitogen-activated protein kinase activity[26]. Our data indicate that increased Ras activity,

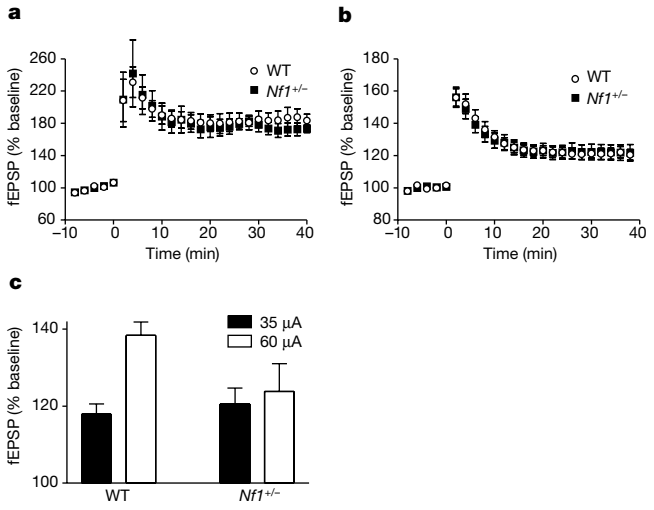

Figure 4 Long-term potentiation deficits in *Nf1*$^{+/-}$ mice are caused by increased inhibition. **a**, LTP induction under picrotoxin using a two-burst induction (wild type (WT), $n = 6$; *Nf1*$^{+/-}$, $n = 5$). **b**, LTP induced with two bursts using a stimulation strength of 35 μA (evokes similar IPSPs in WT and *Nf1*$^{+/-}$ mice, see Fig. 3c) is not different in WT ($n = 13$) and *Nf1*$^{+/-}$ ($n = 16$) mice. **c**, In WT mice the LTP induced at a stimulation strength of 60 μA is larger than LTP induced at 35 μA, whereas in *Nf1*$^{+/-}$ mice it is not (60 μA evokes larger IPSPs in *Nf1*$^{+/-}$ mice).

caused by partial loss of neurofibromin, leads to abnormally high GABA-mediated inhibition, and that this enhancement in inhibition may be responsible for impairments in synaptic plasticity that might underlie the learning deficits associated with NF1. These findings suggest that strategies that decrease either Ras activity or GABA-mediated inhibition might be used to treat the learning deficits associated with NF1. □

Methods

Animals

Generation of the different genetically modified mice has been described[12,27,28]. For the *Nf1*$^{+/-}$/*N-ras*$^{+/-}$ experiment, we generated animals by crossing *Nf1*$^{+/-}$ mice, which had been previously backcrossed five generations to the C57BL/6N background from 129T2/SvEmsJ (N5 into C57BL/6N), with *N-ras*$^{+/-}$ also backcrossed five generations to the C57BL/6N background. All the other animals were 129T2/SvEmsJ–C57BL/6N F_1 hybrids generated by crossing *Nf1*$^{+/-}$ mice (backcrossed more than 11 generations to the C57BL/6N background) with wild-type or *K-ras*$^{+/-}$ mice on the 129T2/SvEmsJ background. Thus, in every experiment the mice from each genotype were littermates and of isogenic genetic background. All experiments were carried out blind with respect to genotype or treatment.

Water maze

The basic protocol for the water maze experiments has been described[10]. Mice from the 129T2/SvEmsJ–C57B/6N F_1 background were given two trials per day (30-s intertrial intervals) with a probe trial (60 s) at the end of training day 7. Because mice from the C57B/6N genetic background take longer to learn the water maze[29], mice from the *Nf1*$^{+/-}$/*N-ras*$^{+/-}$ population (N5 into C57BL/6N) were given three blocks of two trials per day, with a probe trial at training day 5. We used contextual fear conditioning in wild-type mice (129T2/SvEmsJ–C57BL/6N F_1) to determine the dose used in the BMS191563 experiments. With one single injection 6 h before training, a dose of 10 mg per kg (body mass) did not affect learning but higher dosages did (time freezing: saline, 63.3%; 10 mg per kg, 55.8%; 30 mg per kg, 34.4%; 45 mg per kg, 46.7%). But 10 mg per kg injected for 7 days (as in the water maze experiment) affected learning in wild-type mice (saline, 82.9%; 10 mg per kg, 52.2%; $F_{1,10} = 9.43$, $P < 0.05$). As shown, 5 mg per kg injected for 7 days did not affect learning in wild-type mice. We dissolved BMS191563 in sterile saline solution and injected it every day 1 h before the experiment started.

Electrophysiology

For the field potentials, recordings were made from transverse hippocampal slices (400 μm thick) in a submerged recording chamber perfused (2 ml min^{-1}) with artificial cerebrospinal fluid (ACSF) containing (in mM): 120 NaCl, 3.5 KCl, 2.5 $CaCl_2$, 1.3 Mg_2SO_4, 1.25 NaH_2PO_4, 26 $NaHCO_3$ and 10 D-glucose at 30 °C (saturated with 95% O_2 and 5% CO_2). For the LTP experiments, EPSPs were evoked alternatively in separate pathways (control and tetanized) in the CA1 Schaffer collateral/commissural afferents with 100-μs test pulses through two stimulating electrodes (~300 μm from the Pt/Ir recording electrode). Unless indicated otherwise, the stimulation strength in both stimulating electrodes was set to 60 μA. After a 10-min baseline period, LTP was induced in one pathway according to a HFS (100 Hz for 1 s) or TBS protocol (two, five or ten bursts, each burst four pulses at 100 Hz, 200-ms interburst intervals). We excluded from further analysis slices in which there was significant drift in the control pathway or in which seizures developed. The amount of potentiation was calculated as a percentage of the baseline EPSP slope. For the experiments with picrotoxin, the drug was dissolved (10 μM) in ACSF and was present throughout the experiment. For the input–output curves, we applied different stimulation strengths (from 10 to 100 μA in steps of 10 μA). For each slice, five EPSPs were averaged per stimulation strength. Paired-pulse facilitation was assessed by measuring the per cent increase in the slope of the second pulse in relation to the first (20-, 50-, 100-, 200-, 300-, 400-, 500-ms interpulse intervals). The stimulation strength was adjusted to one-third of the maximum EPSP amplitude.

To assess inhibition in *Nf1*$^{+/-}$ mice, we measured IPSPs from CA1 pyramidal neurons using whole-cell (blind technique[30]) bridge mode recordings (Axoclamp 2B, Axon Instruments). IPSPs were evoked through a stimulating electrode placed in the Schaffer collateral/commissural afferents (~75 μm from the recording pipette when AP5 and CNQX were applied) that applied different stimulation strengths (from 10 to 100 μA in steps of 10 μA). The IPSP amplitude was measured, with five IPSPs averaged for each neuron per stimulation strength. The intracellular solution contained (in mM): 135 potassium gluconate, 5 HEPES, 2 Mg^{2+}-ATP, 5 $MgCl_2$, 0.3 GTP, 0.05 EGTA (pipette resistance 7–11 MΩ). To evoke IPSPs monosynaptically, AP5 and CNQX (10 μM) were present in the ACSF.

In all experiments, data were averaged and entered into analysis as a single subject, and therefore reflect individual mice rather than individual slices or neurons.

Statistical analysis

We analysed acquisition data from the water maze by repeated-measures ANOVA. Per cent time in training quadrant for the different genotypes was analysed using single-factor ANOVA; post-hoc comparisons (Fisher's PLSD) between genotypes were carried out when appropriate. Planned comparisons using a paired *t*-test were used to analyse the proximity data. LTP was analysed using single-factor ANOVA on the average amount of LTP 30–40 min after induction. We analysed the inhibition and input–output curves using ANOVA, and post-hoc comparisons were performed when appropriate.

Received 10 August; accepted 21 November 2001.
Published online 16 January 2002, DOI 10.1038/nature711.

1. North, K. Neurofibromatosis type 1. *Am. J. Med. Genet.* **97,** 119–127 (2000).
2. Silva, A. J. *et al.* A mouse model for the learning and memory deficits associated with neurofibromatosis type I. *Nature Genet.* **15,** 281–284 (1997).
3. Ballester, R. *et al.* The *NF1* locus encodes a protein functionally related to mammalian GAP and yeast IRA proteins. *Cell* **63,** 851–859 (1990).
4. Xu, G. F. *et al.* The catalytic domain of the neurofibromatosis type 1 gene product stimulates ras GTPase and complements *ira* mutants of *S. cerevisiae*. *Cell* **63,** 835–841 (1990).
5. Guo, H. F., The, I., Hannan, F., Bernards, A. & Zhong, Y. Requirement of *Drosophila* NF1 for activation of adenylyl cyclase by PACAP38-like neuropeptides. *Science* **276,** 795–798 (1997).
6. Guo, H. F., Tong, J., Hannan, F., Luo, L. & Zhong, Y. A neurofibromatosis-1-regulated pathway is required for learning in *Drosophila*. *Nature* **403,** 895–898 (2000).
7. Xu, H. & Gutmann, D. H. Mutations in the GAP-related domain impair the ability of neurofibromin to associate with microtubules. *Brain Res.* **759,** 149–152 (1997).
8. Ozonoff, S. Cognitive impairment in neurofibromatosis type 1. *Am. J. Med. Genet.* **89,** 45–52 (1999).
9. Morris, R. G., Garrud, P., Rawlins, J. N. & O'Keefe, J. Place navigation impaired in rats with hippocampal lesions. *Nature* **297,** 681–683 (1982).
10. Costa, R. M. *et al.* Learning deficits, but normal development and tumour predisposition, in mice lacking exon 23a of *Nf1*. *Nature Genet.* **27,** 399–405 (2001).
11. Klose, A. *et al.* Selective disactivation of neurofibromin GAP activity in neurofibromatosis type 1. *Hum. Mol. Genet.* **7,** 1261–1268 (1998).
12. Johnson, L. K-r. *et al. ras* is an essential gene in the mouse with partial functional overlap with *N-ras*. *Genes Dev.* **11,** 2468–2481 (1997).
13. Brannan, C. I. *et al.* Targeted disruption of the neurofibromatosis type-1 gene leads to developmental abnormalities in heart and various neural crest-derived tissues. *Genes Dev.* **8,** 1019–1029 (1994).
14. Brandeis, R., Brandys, Y. & Yehuda, S. The use of the Morris water maze in the study of memory and learning. *Int. J. Neurosci.* **48,** 29–69 (1989).
15. Gallagher, M., Burwell, R. & Burchinal, M. Severity of spatial learning impairment in aging: Development of a learning index for performance in the Morris water maze. *Behav. Neurosci.* **107,** 618–626 (1993).
16. Muthalif, M. M. *et al.* Contribution of Ras GTPase/MAP kinase and cytochrome P450 metabolites to deoxycorticosterone-salt-induced hypertension. *Hypertension* **35,** 457–463 (2000).
17. Gibbs, J. B. *et al.* Farnesyltransferase inhibitors versus Ras inhibitors. *Curr. Opin. Chem. Biol.* **1,** 197–203 (1997).
18. Yan, N. *et al.* Farnesyltransferase inhibitors block the neurofibromatosis type I (NF1) malignant phenotype. *Cancer Res.* **55,** 3569–3575 (1995).
19. Kim, H. A., Ling, B. & Ratner, N. Nf1-deficient mouse Schwann cells are angiogenic and invasive and can be induced to hyperproliferate: reversion of some phenotypes by an inhibitor of farnesyl protein transferase. *Mol. Cell. Biol.* **17,** 862–872 (1997).
20. Abbott, L. F. & Nelson, S. B. Synaptic plasticity: taming the beast. *Nature Neurosci.* **3,** 1178–1183 (2000).
21. Larson, J., Wong, D. & Lynch, G. Patterned stimulation at the theta frequency is optimal for the induction of hippocampal long-term potentiation. *Brain Res.* **368,** 347–350 (1986).
22. Hessler, N. A., Shirke, A. M. & Malinow, R. The probability of transmitter release at a mammalian central synapse. *Nature* **366,** 569–572 (1993).
23. Chapman, C. A., Perez, Y. & Lacaille, J. C. Effects of GABAA inhibition on the expression of long-term potentiation in CA1 pyramidal cells are dependent on tetanization parameters. *Hippocampus* **8,** 289–298 (1998).

24. Chorvatova, A., Gendron, L., Bilodeau, L., Gallo-Payet, N. & Payet, M. D. A Ras-dependent chloride current activated by adrenocorticotropin in rat adrenal zona glomerulosa cells. *Endocrinology* **141,** 684–692 (2000).
25. Tong, J. *et al.* NF1-regulated adenylyl cyclase pathway. *Soc. Neurosci. Abstr.* abstract no. 345.9 (Society for Neuroscience, New Orleans, 2000).
26. Ingram, D. A. *et al.* Hyperactivation of p21(ras) and the hematopoietic-specific Rho GTPase, Rac2, cooperate to alter the proliferation of neurofibromin-deficient mast cells in vivo and in vitro. *J. Exp. Med.* **194,** 57–69 (2001).
27. Jacks, T. *et al.* Tumour predisposition in mice heterozygous for a targeted mutation in *Nf1*. *Nature Genet.* **7,** 353–361 (1994).
28. Umanoff, H., Edelmann, W., Pellicer, A. & Kucherlapati, R. The murine *N-ras* gene is not essential for growth and development. *Proc. Natl Acad. Sci. USA* **92,** 1709–1713 (1995).
29. Voikar, V., Koks, S., Vasar, E. & Rauvala, H. Strain and gender differences in the behaviour of mouse lines commonly used in transgenic studies. *Physiol. Behav.* **72,** 271–281 (2001).
30. Blanton, M. G., Lo Turco, J. J. & Kriegstein, A. R. Whole cell recording from neurons in slices of reptilian and mammalian cerebral cortex. *J. Neurosci. Methods* **30,** 203–210 (1989).

Acknowledgements

We thank V. Manne for the BMS191563, and E. Friedman for technical assistance in earlier experiments. We are grateful to M. Barad, D. Buonomano, T. Cannon, J. Colicelli, P. Frankland, L. Kaczmarek, A. Matynia, M. Sanders and D. Smith for discussions, and to C. Brannan and S. Schlussel for encouragement. R.M.C. received support from the Graduated Program in Basic and Applied Biology (GABBA) of the University of Oporto, the Portuguese Foundation for Science and Technology (FCT) and the National Neurofibromatosis Foundation (NNF). This work was also supported by a generous donation from K. M. Spivak, and by grants from the NIH (R01 NS38480), Neurofibromatosis Inc. (National, Illinois, Mass Bay Area, Minnesota, Arizona, Kansas and Central Plains, Mid-Atlantic, and Texas chapters), the Merck and the NNF foundations to A.J.S.

Competing interests statement

The authors declare that they have no competing financial interests.

Correspondence and requests for materials should be addressed to A.J.S. (e-mail: Silvaa@mednet.ucla.edu).

Gene expression profiling predicts clinical outcome of breast cancer

Laura J. van 't Veer*†, Hongyue Dai†‡, Marc J. van de Vijver*†, Yudong D. He‡, Augustinus A. M. Hart*, Mao Mao‡, Hans L. Peterse*, Karin van der Kooy*, Matthew J. Marton‡, Anke T. Witteveen*, George J. Schreiber‡, Ron M. Kerkhoven*, Chris Roberts‡, Peter S. Linsley‡, René Bernards* & Stephen H. Friend‡

** Divisions of Diagnostic Oncology, Radiotherapy and Molecular Carcinogenesis and Center for Biomedical Genetics, The Netherlands Cancer Institute, 121 Plesmanlaan, 1066 CX Amsterdam, The Netherlands*
‡ Rosetta Inpharmatics, 12040 115th Avenue NE, Kirkland, Washington 98034, USA
† These authors contributed equally to this work

Breast cancer patients with the same stage of disease can have markedly different treatment responses and overall outcome. The strongest predictors for metastases (for example, lymph node status and histological grade) fail to classify accurately breast tumours according to their clinical behaviour[1–3]. Chemotherapy or hormonal therapy reduces the risk of distant metastases by approximately one-third; however, 70–80% of patients receiving this treatment would have survived without it[4,5]. None of the signatures of breast cancer gene expression reported to date[6–12] allow for patient-tailored therapy strategies. Here we used DNA microarray analysis on primary breast tumours of 117 young patients, and applied supervised classification to identify a gene expression signature strongly predictive of a short interval to distant metastases ('poor prognosis' signature) in patients without tumour cells in local lymph nodes at diagnosis (lymph node negative). In addition, we established a signature that identifies tumours of *BRCA1* carriers. The poor prognosis signature consists of genes regulating cell cycle, invasion, metastasis and angiogenesis. This gene expression profile will outperform all currently used clinical parameters in predicting disease outcome. Our findings provide a strategy to select patients who would benefit from adjuvant therapy.

We selected 98 primary breast cancers: 34 from patients who developed distant metastases within 5 years, 44 from patients who continued to be disease-free after a period of at least 5 years, 18 from patients with *BRCA1* germline mutations, and 2 from *BRCA2* carriers. All 'sporadic' patients were lymph node negative, and under 55 years of age at diagnosis. From each patient, 5 μg total RNA was isolated from snap-frozen tumour material and used to derive complementary RNA (cRNA). A reference cRNA pool was made by pooling equal amounts of cRNA from each of the sporadic carcinomas. Two hybridizations were carried out for each tumour using a fluorescent dye reversal technique on microarrays containing approximately 25,000 human genes synthesized by inkjet technology[13]. Fluorescence intensities of scanned images were quantified, normalized and corrected to yield the transcript abundance of a gene as an intensity ratio with respect to that of the signal of the reference pool[14]. Some 5,000 genes were significantly regulated across the group of samples (that is, at least a twofold difference and a *P*-value of less than 0.01 in more than five tumours).

An unsupervised, hierarchical clustering algorithm allowed us to cluster the 98 tumours on the basis of their similarities measured over these approximately 5,000 significant genes. Similarly, the ~5,000 genes were clustered on the basis of their similarities measured over the group of 98 tumours (Fig. 1a). In the dendrograms shown in Fig. 1a (left and top), the length and the subdivision of the branches displays the relatedness of the breast tumours (left) and the expression of the genes (top). Two distinct groups of tumours are the dominant feature in this two-dimensional display (top and bottom of plot, representing 62 and 36 tumours, respectively), suggesting that the tumours can be divided into two types on the basis of this set of ~5,000 significant genes. Notably, in the upper group only 34% of the sporadic patients were from the group who developed distant metastases within 5 years, whereas in the lower group 70% of the sporadic patients had progressive disease (Fig. 1b). Thus, using unsupervised clustering we can already, to some extent, distinguish between 'good prognosis' and 'poor prognosis' tumours.

To gain insight into the genes of the dominant expression signatures, we associated them with histopathological data; for example, oestrogen receptor (ER)-α expression as determined by immunohistochemical (IHC) staining (Fig. 1b). Out of 39 IHC-stained tumours negative for ER-α expression (ER negative), 34 clustered together in the bottom branch of the tumour dendrogram. In the enlargement shown in Fig. 1c, a group of downregulated genes is represented containing both the ER-α gene *(ESR1)* and genes that are apparently co-regulated with ER, some of which are known ER target genes. A second dominant gene cluster is associated with lymphocytic infiltrate and includes several genes expressed primarily by B and T cells (Fig. 1d).

Sixteen out of eighteen tumours of *BRCA1* carriers are found in the bottom branch intermingled with sporadic tumours. This is consistent with the idea that most *BRCA1* mutant tumours are ER negative and manifest a higher amount of lymphocytic infiltrate[15]. The two tumours of *BRCA2* carriers are part of the upper cluster of tumours and do not show similarity with *BRCA1* tumours. Neither high histological grade nor angioinvasion is a specific feature of either of the clusters (Fig. 1b). We conclude that unsupervised clustering detects two subgroups of breast cancers, which differ in ER status and lymphocytic infiltration. A similar conclusion has also been reported previously[7,16].

The 78 sporadic lymph-node-negative patients were selected specifically to search for a prognostic signature in their gene expression profiles. Forty-four patients remained free of disease